Enhanced Laser-Driven Ion Acceleration in the Relativistic Transparency Regime

A. Henig,[1,2,*] D. Kiefer,[1,2] K. Markey,[3] D. C. Gautier,[4] K. A. Flippo,[4] S. Letzring,[4] R. P. Johnson,[4] T. Shimada,[4] L. Yin,[4] B. J. Albright,[4] K. J. Bowers,[4] J. C. Fernández,[4] S. G. Rykovanov,[1,5] H.-C. Wu,[1] M. Zepf,[3] D. Jung,[1,2] V. Kh. Liechtenstein,[6,2] J. Schreiber,[1,2,7] D. Habs,[1,2] and B. M. Hegelich[2,4]

[1]*Max-Planck-Institut für Quantenoptik, Garching, Germany*
[2]*Department für Physik, Ludwig-Maximilians-Universität München, Garching, Germany*
[3]*Department of Physics and Astronomy, Queens University Belfast, BT7 1NN, United Kingdom*
[4]*Los Alamos National Laboratory, Los Alamos, New Mexico 87545, USA*
[5]*Moscow Engineering Physics Institute, Kashirskoe shosse 31, Moscow, Russia*
[6]*RRC "Kurchatov Institute," 123182, Moscow, Russia*
[7]*Plasma Physics Group, Blackett Laboratory, Imperial College London, SW7 2BZ, United Kingdom*

(Received 18 January 2009; published 21 July 2009)

We report on the acceleration of ion beams from ultrathin diamondlike carbon foils of thickness 50, 30, and 10 nm irradiated by ultrahigh contrast laser pulses at intensities of $\sim 7 \times 10^{19}$ W/cm^2. An unprecedented maximum energy of 185 MeV (15 MeV/u) for fully ionized carbon atoms is observed at the optimum thickness of 30 nm. The enhanced acceleration is attributed to self-induced transparency, leading to strong volumetric heating of the classically overdense electron population in the bulk of the target. Our experimental results are supported by both particle-in-cell (PIC) simulations and an analytical model.

DOI: 10.1103/PhysRevLett.103.045002 PACS numbers: 52.38.Kd, 41.75.Jv, 52.50.Jm, 52.65.Rr

Acceleration of ions by intense laser-plasma interactions has attracted increasing interest over the last few years, constituting a rapidly evolving field of research. In past experiments, μm-scale thin foils were used as target material to generate multi-MeV, high-quality ion beams. The predominant mechanism in that case was found to be target normal sheath acceleration (TNSA [1]). In this scenario, the incident intense laser pulse strongly heats electrons situated at the front surface of the opaque target. Such relativistic electrons cross the target to set up an electric field with magnitude exceeding 1 TV/m at the nonirradiated side. Atoms located in the substrate and in surface layers, which are formed by contaminations of hydrocarbons and H_2O, become ionized and subsequently accelerated. It is evident, that particles with high charge-to-mass (q/m) ratio, i.e., protons, will favorably gain energy from the sheath field, which results in a considerable reduction in acceleration for other ion species. By virtue of this mechanism, proton beams of energies up to 60 MeV have been demonstrated [2]. In order to efficiently accelerate heavier ions by employing TNSA, hydrogen contaminants need to be removed from the target [3–5]. It has been shown that this is most effectively done by resistive heating, yielding medium-mass ion cutoff energies of $\sim$3.5 MeV/u for carbon C^{5+} [4] and 5 MeV/u for fluorine F^{7+} [3].

For TNSA, the use of thin foils proved to be most efficient for ion acceleration [6], which is confirmed by the models available so far [2,7,8]. However, it has been demonstrated in previous work that for TNSA an optimum foil thickness exists for a given laser contrast, pulse duration, and intensity [9]. This lower limit is given by the restriction that the shock wave launched at the target front side by the ASE pedestal and prepulses must not have time to reach the target back to perturb the acceleration. Theoretical studies have predicted an enhanced acceleration when a submicron foil target is irradiated under ultrahigh contrast [10–14]. As opposed to conventional TNSA where the target remains opaque, the foil becomes relativistically transparent during the interaction [14–16]. This leads to strong volumetric heating of the bulk electrons and, consequently, increased electrostatic fields. So far, ion acceleration from ultrathin foils has been experimentally restricted to intensities of 1×10^{19} W/cm^2 and below, as well as maximum pulse energies of 1 J on targets down to 20 nm in thickness [17–19]. With these parameters being orders of magnitude smaller than necessary for enhanced ion acceleration in the transparency regime, only ion beams accelerated by TNSA from opaque foils have been demonstrated up to now using such targets.

In this Letter, we report for the first time on the acceleration of proton and carbon beams from ultrathin, diamondlike carbon (DLC) foils of 50, 30 and 10 nm thickness irradiated with high-contrast pulses at significantly increased intensities of $\sim 7 \times 10^{19}$ W/cm^2. At the optimum foil thickness of 30 nm, carbon ions reach cutoff energies of 185 MeV (15 MeV/u) which is a factor of 3 higher than reported so far. The strong energy transfer from the electric field of the laser to the ions is attributed to an enhanced acceleration field, owing to relativistic transparency and subsequent volumetric heating of the target electrons as illustrated above. Our interpretations are con-

firmed by one- and two-dimensional particle-in-cell (PIC) simulations. In addition, a simple analytical model is presented to predict the optimum thickness for given laser parameters, demonstrating the direct connection between the instantaneous laser intensity at the time when the target becomes relativistically transparent and the resulting maximum ion energies.

The experiments we present here were conducted at the TRIDENT laser facility at Los Alamos National Laboratory (LANL). The employed 100 TW short pulse beam delivers 80 J pulses compressed to 700 fs at a central wavelength of 1053 nm. The initial contrast, i.e., the relative intensity of the amplified spontaneous emission (ASE)-pedestal arriving ~400 ps prior to the main peak, was determined to be $\sim 10^{-8}$. In order to further enhance that value, two antireflection coated glass slides ($R < 0.5\%$) were introduced into the converging beam after reflection of a $f/3.5$ off-axis parabolic mirror (Fig. 1). Each glass was placed at around 45° angle of incidence at intensities of 5×10^{14} W/cm^2 and 2×10^{15} W/cm^2, respectively. Thus, the ASE pedestal and prepulses were kept below the ionization threshold and therefore transmitted, while the main pulse was reflected of the dense plasma surface created by its own rising edge [20]. By use of this double-plasma mirror technique, a ps–time-scale pulse contrast of $\sim 10^{-12}$ was achieved. The laser energy after the double reflection was measured to be 40–50 J, depending on the input polarization, resulting in peak intensities of $\sim 7 \times 10^{19}$ W/cm^2–9×10^{19} W/cm^2 in a 10 μm FWHM diameter focal spot. DLC foil targets of thicknesses 50, 30, and 10 nm, free-standing over a diameter of 1 mm, were placed at the focus and irradiated under normal incidence. DLC is a metastable form of amorphous carbon containing a significant portion of sp3-bonded atoms in the matrix, giving DLC its diamondlike properties. Compared to other materials available, the optically nearly transparent DLC foils offer an exceptionally high tensile strength, hardness, and heat resistance, making DLC an ideally suited material for ultrathin self-supporting targets. For the presented experiment we used foils with a fraction of ~50% sp3 bonds and a density of 2.2 g/cm^3 produced by a modified dc glow discharge sputtering technique [21]. To characterize the accelerated particles, two complementary diagnostics were implemented behind the target: (i) a 5×5 cm stack of radiochromic films (RCF) separated 4 cm from the target to obtain the angular distribution of the emitted proton beam, (ii) a Thomson parabola spectrometer at a distance of 97.5 cm (solid angle $\sim 3.3 \times 10^{-8}$ sr) to detect particles propagating along the target normal, that were transmitted through a hole of diameter 4 mm located in the RCF stack center. At the back of the spectrometer, CR39 nuclear track detectors of 1 mm thickness were positioned, capable to stop and thus record traces of ions ranging in energy from ~100 keV up to ~10 MeV for protons and ~210 MeV for carbon ions, respectively. To extend the detection interval to higher energy ions with ranges above 1 mm, an image plate covered by a 15 μm aluminum foil was placed behind the CR39 plate.

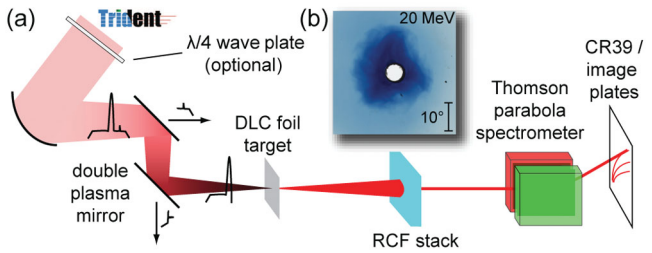

FIG. 1 (color). Experimental setup at TRIDENT (a) and a characteristic image of the proton beam profile at 20 MeV energy as obtained from a 50 nm DLC target (b).

Irradiating a 50 nm DLC target with a linearly polarized pulse at high contrast, we obtained a maximum proton energy of 25 MeV. The corresponding beam profiles as seen on the RCF stack [Fig. 1(b)] showed a homogenous angular distribution with opening angles of ~30° for 20 MeV and ~18° for 25 MeV protons. Additionally, traces of carbon ions covering all charge states from C^{1+} to C^{6+} were detected on the CR39. The broad energy distribution of fully ionized carbon extended to 157 MeV [Fig. 2(a)]. Both the cutoff value, i.e., the ion energy where the observed number of particles equals the noise level, as well as the spectral shape were closely reproduced when the laser polarization was changed to circular before the double-plasma mirror by passing the beam through a potassium dihydrogen phosphate (KDP) crystal operating as $\lambda/4$ wave plate. Owing to the stronger absorption of p-polarized components of laser light reflected from plasma, the target was irradiated by an elliptically polarized beam in this configuration. We estimated the elliptic-

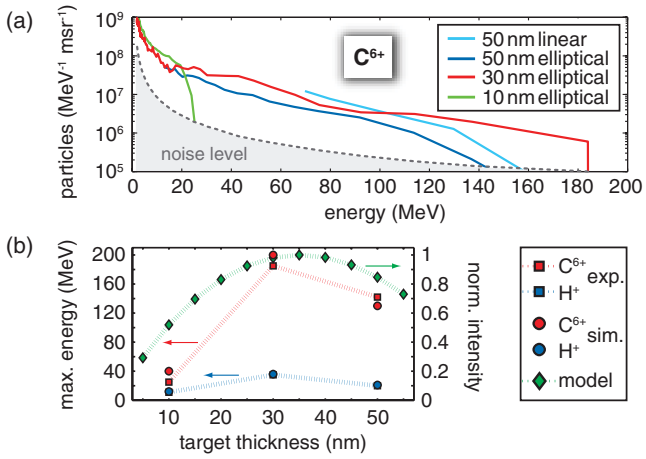

FIG. 2 (color). Observed spectra of fully ionized carbon ions (a) for foil thicknesses of 50, 30, and 10 nm. An optimum in acceleration is seen for the 30 nm target, in excellent agreement with maximum energies of C^{6+} and protons deduced from 1D PIC simulations (b). The normalized instantaneous laser intensity at burnthrough time as derived from the presented analytical model (green diamonds) closely follows the cutoff energy curve.

ity, i.e., the ratio between the p- and s-polarized fraction of the laser electric field, by 1D PIC simulations to be $\epsilon = 0.5$. Comparing the spectra of C^{6+} for varying DLC-foil thicknesses from 50 nm down to 10 nm, a distinct maximum in cutoff energy was observed for irradiation of a 30 nm target [Fig. 2(a)]. Here, the distribution reached up to 185 MeV. Lower charge states were detected at significantly reduced energies below 20 MeV, showing no noticeable dependence on target thickness. The proton spectra also exhibited an optimum at the foil thickness of 30 nm, reaching values of 35 MeV, while 50 and 10 nm gave 20 and 11 MeV, respectively [Fig. 2(b)].

To aid the understanding of the experimental findings, 1D and 2D PIC simulations were carried out employing the VPIC code [22]. Solid density (2.2 g/cm^3; $n_e/n_{\rm cr} = 660$) C^{6+} targets, 10, 30, and 50 nm thick mixed with 20% protons (in number density), are considered. Here, n_e stands for the electron density, whereas $n_{\rm cr} = \epsilon_0 m_e \omega_L^2/e^2$ denotes the critical density of the plasma with electron mass m_e and laser carrier frequency ω_L. A linearly polarized pulse of intensity $I(t) = I_0 \sin^2(t\pi/\tau)$ with $I_0 = 7 \times 10^{19}$ W/cm^2 and $\tau = 1400$ fs (FWHM 700 fs) is used to model the TRIDENT laser. The simulation domain is 100 μm long in 1D and 50 μm in both laser (x) and transverse (z) direction in 2D. The cell size is $0.3\lambda_D^0$ with 167×10^3 particles per cell in 1D and $0.4\lambda_D^0$ along x and $1.6\lambda_D^0$ along z with 500 particles per cell in 2D (λ_D^0 is the initial Debye length; the initial electron temperature is $T_e = 165$ keV). A comparison of 1D PIC simulation and experimental results on C^{6+} and proton cutoff energies is presented in Fig. 2(b). For each foil thickness, the experimentally obtained maximum energies of both ion species are closely reproduced.

Calculating the collisional skin depth, i.e., the decay length $l_s \simeq c/\omega_p$ of the evanescent field in the initially highly overdense plasma layer where ω_p is the Langmuir frequency $\omega_p = (n_e e^2/\epsilon_0 m_e)^{1/2}$, we obtain $l_s \sim 6.2$ nm. Thus, even the thinnest, 10 nm DLC foil is opaque to the incident laser beam at the beginning of the interaction. However, the simulations show that within the laser pulse duration each of the three targets becomes relativistically transparent to the laser electric field eventually. In Fig. 3, we use a 2D simulation of the 10 nm target case to demonstrate the effects of relativistic transparency. The black curve in Fig. 3(a) is the electron density $n_e/n_{\rm cr}$ at a time $t_1 = -355$ fs prior to the peak of the pulse, when the laser beam has just penetrated the target. Up to this point in time, the target has expanded to a thickness comparable to the laser wavelength with a peak density $n_e/n_{\rm cr} \sim 6.8$. Accounting for relativistic effects, the peak density normalized over the corrected critical density $n_e/(n_{\rm cr}\gamma) \sim 1$, where $\gamma \sim 6.8$ was obtained from the simulation as an average over electrons situated at the spatial location of the peak density, and the target becomes marginally underdense. Strong volumetric heating of electrons located in the bulk of the foil sets in, driven by the laser pulse penetrating

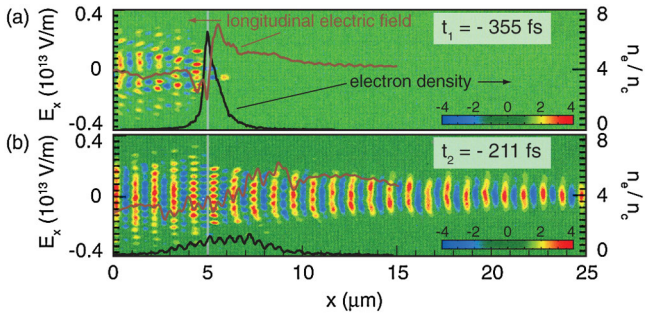

FIG. 3 (color). Electric field in y direction as deduced from a 2D PIC simulation at times $t_1 = -355$ fs (a) and $t_2 = -211$ fs (b) before the peak of the laser pulse reaches the 10 nm target initially located at $x = 5$ μm (color scale given in units of 10^{13} V/m). The black curve shows the normalized electron density $n_e/n_{\rm cr}$, while the longitudinal electric field E_x is marked in red. Each quantity represents an average over 2 μm in transverse (z) direction around the focal spot center.

the target. Subsequently, rapid ion acceleration follows as the C^{6+} ions comove with the localized enhancement in the electric field E_x, shown by the red curve in Fig. 3(a). This stage lasts until the target thickness increases to several microns and the peak density $n_e/n_{\rm cr}$ reduces to unity, as captured by the black curve in Fig. 3(b). During this time interval, the carbon ions and protons gain the major fraction of their energy and reach their respective maximum of 40 and 11 MeV.

However, the 10 nm target becomes transparent to the laser at a time much before the laser intensity has evolved to its peak. Consequently, the short period of strong ion acceleration between times t_1 when the target becomes relativistically transparent [$n_e/(n_{\rm cr}\gamma) \sim 1$] and t_2 when the electron density dropped to the critical density ($n_e/n_{\rm cr} \sim 1$) takes place at the early rising edge of the laser pulse. Already at $t_2 = -211$ fs before the pulse maximum reaches the target, the acceleration of ions is terminated. On the other hand, the 50 nm target becomes transparent near the end of the laser pulse. The 30 nm target becomes transparent when the intensity is closer to the peak; in this case the transfer of laser energy into electric field energy is maximized, resulting in the highest ion energies. This major outcome is confirmed by predictions from a simple analytical model starting from the first law of thermodynamics

$$\varepsilon I(t)dt = \tfrac{3}{2} n_{e,0} L_0 dT_e + n_e(t) T_e(t) dL, \qquad (1)$$

where the left-hand side represents the laser energy absorption into electrons with efficiency ε. The first term on the right-hand side describes the resulting change in electron temperature, while the second includes the longitudinal plasma expansion. A common factor of spot size area has been divided from all terms. If we assume a longitudinal self-similar plasma expansion at the ion sound speed $c_s = [\frac{5}{3} Z_i T_e(t)/m_i]^{1/2}$, i.e., that $n_e(t) = n_{e,0} L_0/L(t)$,

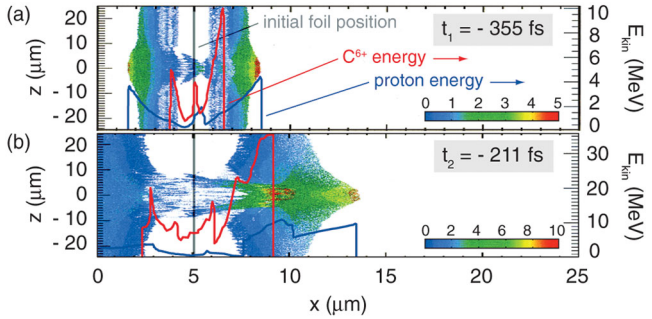

FIG. 4 (color). Two-dimensional spatial distribution of proton energies as seen in a 2D PIC simulation of a 10 nm foil at times $t_1 = -355$ fs (a) and $t_2 = -211$ fs (b) before the arrival of the main pulse at the target (color scale given in units of MeV). Overlaid are the proton energies (blue curve) and the C^{6+} energies (red curve) at $z = 0$.

where the thickness $L(t)$ evolves as $L(t) = L_0 + \int_0^t dt' c_s(t')$, then we can obtain $T_e(t)$ numerically from a nonlinear ordinary differential equation (ODE). Burnthrough of the target occurs when $n_e(t) \approx \gamma n_{cr}$, where $\gamma = 1 + 3T_e(t)/(2m_e c^2)$. A more detailed description of the model will be given in a separate publication elsewhere. The instantaneous laser intensity (normalized to peak intensity) at burnthrough time [i.e., $I(t_1)$] as derived from the model with $\varepsilon = 0.04$, which is low owing to the small target thicknesses used [11], has been overlaid in Fig. 2(b) for different target thicknesses L_0. The dependency of the ion maximum energy on initial target thickness is closely reproduced by the corresponding burnthrough intensity curve resulting from the model, thus verifying the direct connection between the two quantities. With given laser conditions, an optimal target thickness exists such that the laser pulse is near its maximum intensity at the time the target becomes transparent to the laser.

Figure 4 shows the spatial distribution of proton energies in two dimensions as resulting from the simulation of a 10 nm target and, in addition, the proton energies (blue curve) and the C^{6+} energies (red curve) at the focal spot center ($z = 0$). Ions accelerated in forward direction obtain significantly higher energies than the ones moving backwards, with the component originating from the target back surface being dominant over the fraction from the front. This behavior differs from the adiabatic expansion described in [23] where shorter pulses (<100 fs) focused to comparable intensities are considered, leading to a symmetric acceleration that happens primarily after the end of the laser pulse.

In summary, we have presented experimental results on proton and carbon ion acceleration from ultrathin DLC foils of 50, 30, and 10 nm thickness. A distinct maximum in the ion cutoff energies is observed using a 30 nm target. As compared to conventional TNSA, which is dominant for opaque foils, the acceleration of ions is drastically enhanced, resulting in unprecedented C^{6+} cutoff energies up to 185 MeV. This increase is attributed to a large longitudinal electric field, generated by strong volumetric heating of the electrons in the bulk when self-induced transparency enables the laser beam to penetrate the target; moreover, this localized field comoves with the C^{6+} ions, resulting in rapid ion acceleration [14]. In previous work, a lower limit for the foil thickness was imposed by the shock wave generated from imperfect laser contrast. We demonstrate for the first time experimentally that such a limit also exists when high-contrast pulses are used because target transparency arises before the peak intensity of the laser pulse, resulting in a lower longitudinal field and decreased total absorption. Raising the maximum energies achievable in laser-driven ion acceleration represents a major step towards parameters necessary for potential applications. Those range from ion-assisted fast ignition inertial confinement fusion (ICF) to oncology and hadron therapy of tumors.

We thank J. Meyer-ter-Vehn for fruitful discussions. This work was performed under the auspices of the U.S. DOE and was supported by the LANL LDRD program and by the DFG under Contract No. TR18 and the DFG cluster of excellence MAP. A. Henig, D. Kiefer, D. Jung, and S. G. Rykovanov acknowledge financial support from IMPRS-APS, J. Schreiber from DAAD.

*andreas.henig@mpq.mpg.de

[1] S. C. Wilks *et al.*, Phys. Plasmas **8**, 542 (2001).
[2] L. Robson *et al.*, Nature Phys. **3**, 58 (2007).
[3] M. Hegelich *et al.*, Phys. Rev. Lett. **89**, 085002 (2002).
[4] B. M. Hegelich *et al.*, Nature (London) **439**, 441 (2006).
[5] P. McKenna *et al.*, Plasma Phys. Controlled Fusion **49**, B223 (2007).
[6] A. J. Mackinnon *et al.*, Phys. Rev. Lett. **88**, 215006 (2002).
[7] J. Fuchs *et al.*, Nature Phys. **2**, 48 (2006).
[8] J. Schreiber *et al.*, Phys. Rev. Lett. **97**, 045005 (2006).
[9] M. Kaluza *et al.*, Phys. Rev. Lett. **93**, 045003 (2004).
[10] Q. L. Dong *et al.*, Phys. Rev. E **68**, 026408 (2003).
[11] E. d'Humières *et al.*, Phys. Plasmas **12**, 062704 (2005).
[12] T. Esirkepov, M. Yamagiwa, and T. Tajima, Phys. Rev. Lett. **96**, 105001 (2006).
[13] L. Yin *et al.*, Laser Part. Beams **24**, 291 (2006).
[14] L. Yin *et al.*, Phys. Plasmas **14**, 056706 (2007).
[15] V. A. Vshivkov *et al.*, Phys. Plasmas **5**, 2727 (1998).
[16] J. Fuchs *et al.*, Phys. Rev. Lett. **80**, 2326 (1998).
[17] D. Neely *et al.*, Appl. Phys. Lett. **89**, 021502 (2006).
[18] P. Antici *et al.*, Phys. Plasmas **14**, 030701 (2007).
[19] T. Ceccotti *et al.*, Phys. Rev. Lett. **99**, 185002 (2007).
[20] H. C. Kapteyn *et al.*, Opt. Lett. **16**, 490 (1991).
[21] V. K. Liechtenstein *et al.*, Nucl. Instrum. Methods Phys. Res., Sect. A **397**, 140 (1997).
[22] K. J. Bowers *et al.*, Phys. Plasmas **15**, 055703 (2008).
[23] A. Andreev *et al.*, Phys. Rev. Lett. **101**, 155002 (2008).